Chinese Chemical Letters 32 (2021) 765–769

Contents lists available at ScienceDirect

Chinese Chemical Letters

journal homepage: www.elsevier.com/locate/cclet

Communication

Molybdenum-doped titanium dioxide supported low-Pt electrocatalyst for highly efficient and stable hydrogen evolution reaction

Ke Chen, Shaofeng Deng, Yun Lu, Mingxing Gong, Yezhou Hu, Tonghui Zhao, Tao Shen, Deli Wang*

Key Laboratory of Material Chemistry for Energy Conversion and Storage (Huazhong University of Science and Technology), Ministry of Education, Hubei Key Laboratory of Material Chemistry and Service Failure, School of Chemistry and Chemical Engineering, Huazhong University of Science and Technology, Wuhan 430074, China

ARTICLE INFO

Article history:
Received 11 April 2020
Received in revised form 6 May 2020
Accepted 21 May 2020
Available online 23 May 2020

Keywords:
Low-Pt electrocatalyst
Oxide support
Strong metal-support interaction
Hydrogen spillover effect
Hydrogen evolution reaction

ABSTRACT

The Platinum (Pt)-based catalysts exhibit excellent catalytic performance for the hydrogen evolution reaction (HER) while suffering from poor stability due to the weak interaction between the carbon support and Pt. Herein, a molybdenum-doped titanium dioxide ($Ti_{0.9}Mo_{0.1}O_2$) supported low-Pt electrocatalyst with stronger interaction between catalyst and support is applied to tune the electrocatalytic performance of Pt. The $Ti_{0.9}Mo_{0.1}O_2$ support can not only tolerate the corrosion environment in the catalytic system, but also generate strong metal-support interaction (SMSI) between the oxide and catalyst. A facile solvothermal method is used to prepare $Ti_{0.9}Mo_{0.1}O_2$ as support to anchor Pt nanoparticles. The 5% Pt supported on $Ti_{0.9}Mo_{0.1}O_2$ catalyst exhibits 4.4-fold mass activity (MA) at an overpotential of 50 mV and higher stability than 20% Pt/C with only 1/4 Pt loading. The SMSI between the $Ti_{0.9}Mo_{0.1}O_2$ and Pt prevents the Pt aggregation to achieve excellent stability, and hydrogen spillover effect in the interface between Pt and support benefits the hydrogen production process. This work presents a novel sight for the fabrication and design of oxide supported catalysts in various catalytic system by reasonably employing support effect.

Hydrogen energy has aroused tremendous attention in face of the depletion of fossil fuels because of its cleanness and high energy density [1–4]. High purity hydrogen can be produced by electrochemical water splitting, which is constitutive of hydrogen evolution reaction (HER) and oxygen evolution reaction (OER). The HER process is highly dependent on the electrocatalyst to overcome the inherent thermodynamic overpotential and increase the energy conversion efficiency. Up to now, Platinum (Pt)-based materials have been universally regarded as the most active catalysts for HER. However, the exceeding insufficiency of Pt resources has rapidly elevated its price, which limits its large-scale application. An alternative way to lower the cost of catalysts is to reduce the use of Pt in the catalysts. For example, loading Pt on the support can improve the dispersion and the utilization of particles by exposing more active sites. Nowadays, the most commonly used support of Pt-based catalyst are carbon-based materials, which possess excellent electrical conductivity as well as large specific surface area. Nevertheless, the weak interaction between carbon and Pt easily lead to the agglomeration or shedding of catalyst particles in operating conditions, resulting in reduced catalytic service life [5]. A desirable catalyst support not only need excellent conductivity, superior physicochemical stability and low cost, but also requires strong interaction between catalyst and support. Therefore, it is necessary to explore new supports with stronger interaction with catalyst to achieve better stability [6–8].

Metal oxide is a promising substitute for the carbon-based support owing to its low cost, nontoxicity, excellent mechanical strength and chemical stability. To date, several transition metal oxides (including TiO_2 [9], CeO_2 [10], WO_x [11], SnO_2 [12]) have been developed as alternative supports in electrochemical reactions, especially for TiO_2, which have attracted enormous attentions. It has been reported that TiO_2 can generate strong metal to support interaction (SMSI) with the supported metal catalyst [13,14]. The SMSI induced charge transfer effect enhances the interaction between the metal and support [15,16]. However, there are several obstacles hindering the application of TiO_2 support in

* Corresponding author.
E-mail address: wangdl81125@hust.edu.cn (D. Wang).

https://doi.org/10.1016/j.cclet.2020.05.030

electrocatalytic system. Most importantly, TiO_2 is a typical semiconductor material with a high band gap [17,18], however, its inherent low conductivity severely limits its application as an electrocatalyst support. To address these issues, there are some traditional methods including metal atom doping, partial reduction of Ti into Magnéli phase [19,20] or composite with conductive materials [21–24]. Heteroatom doping is a facile and effective method to improve the conductivity. Researchers have reported such materials including doped elements such as Nb [25,26], Mo [27], W [28], Ru [29], Ta [30], *etc.* Recently, Tsai [31] and co-workers reported Mo-doped titanium dioxide as the support for Pt nanoparticles which exhibited enhanced mass activity and stability for the oxygen reduction reaction. The electron transfer from the Mo-doped titanium dioxide to Pt induced by SMSI could be explained for the improved catalytic performance.

The hydrogen spillover effect has also been reported to enhance the HER performance [11,32–34], and it is very common in supported metal nanoparticles where the absorbed H atom migrate from the surface of strong binding sites (metal) to that of weak binding sites (support). A study on single atom Pt supported on WO_{3-x} (Pt SA/WO_{3-x}) showed that the hydrogen spillover effect between the tungsten oxide and Pt enhanced the HER catalytic activity [11]. In this case, hydrogen insertion/extraction behavior would be expedited due to the rapid re-exposure of the Pt surface. Under the circumstance, we intend to explore the possibility of applying TiO_2-based materials as HER catalyst support. Besides, there are rare reports about TiO_2-based supports applied in HER [35].

Herein, molybdenum-doped titanium oxide ($Ti_{0.9}Mo_{0.1}O_2$) has been prepared as support to anchor Pt nanoparticles with low metal loading of 5 wt%. Spectroscopy characterization confirms the SMSI effect between the catalyst and support. Combining with hydrogen spillover effect, the Pt/$Ti_{0.9}Mo_{0.1}O_2$ catalyst exhibits 4.4 times higher mass activity and more excellent durability over 10,000 cycles than 20% Pt/C catalyst. The SMSI between the Pt and the $Ti_{0.9}Mo_{0.1}O_2$ enhance the dispersion of the catalyst particles, the hydrogen spillover effect make it faster for the re-exposure of the active surface of Pt, thus improving the utilization of the Pt and achieving excellent stability.

Fig. 1a shows the X-ray diffraction (XRD) patterns of Pt/$Ti_{0.9}Mo_{0.1}O_2$, $Ti_{0.9}Mo_{0.1}O_2$ and TiO_2. The $Ti_{0.9}Mo_{0.1}O_2$ support exhibits amorphous structure while the TiO_2 prepared with similar methods exhibits the crystal structure of anatase titanium dioxide (PDF card 01-071-1167). No signal corresponding to the phase of Mo metal/oxides were observed due to the low content of Mo. As shown in Fig. S1 (Supporting information), the Pt/$Ti_xMo_{1-x}O_2$ with different Mo content and Pt/MoO_2 exhibits similar crystal structure with amorphous support, demonstrating that the structure transformation of TiO_2 is possibly due to the Mo doping. After the deposition of Pt, the Pt/$Ti_{0.9}Mo_{0.1}O_2$ exhibits typical diffraction peaks centered at 39.6°, 46.1°, 67.2° and 80.9°, which are assigned to the (111), (200), (220), (311) plane for face-center cubic Pt (PDF card 01-087-0640), indicating the successful loading of Pt onto the amorphous $Ti_{0.9}Mo_{0.1}O_2$.

Raman spectroscopy was conducted to reveal the structure of catalysts as shown in Fig. 1b. All the catalysts exhibit the same peaks located at 150 cm^{-1} (E_g), 396 cm^{-1} (B_{1g}), 636 cm^{-1} (E_g), suggesting the existence of TiO_2. An additional peak located at 993 cm^{-1} was observed in both the Pt/$Ti_{0.9}Mo_{0.1}O_2$ and $Ti_{0.9}Mo_{0.1}O_2$, which is attributed to the stretching vibration of Mo=O for molybdenum oxide [31]. This result further demonstrate the successful doping of Mo into TiO_2. From the inset in Fig. 1b, the peaks at 150 cm^{-1} for Pt/$Ti_{0.9}Mo_{0.1}O_2$ are obviously shifted to higher Raman shift after anchoring Pt onto the $Ti_{0.9}Mo_{0.1}O_2$ support, which verifies the interaction between $Ti_{0.9}Mo_{0.1}O_2$ support and Pt. And two obvious peaks at around 1350 cm^{-1} and 1580 cm^{-1} are characteristic for the D-band and G-band of carbon materials, respectively. The existence of carbon in $Ti_{0.9}Mo_{0.1}O_2$ is due to the carbonization of glycerate formed in solvothermal process. As a matter of fact, the residual carbon in $Ti_{0.9}Mo_{0.1}O_2$ support is beneficial for the conductivity of the catalyst.

The morphology of the synthesized $Ti_{0.9}Mo_{0.1}O_2$ and Pt/$Ti_{0.9}Mo_{0.1}O_2$ was examined by scanning electron microscopy (SEM) in Fig. S2 (Supporting information). The $Ti_{0.9}Mo_{0.1}O_2$ shows a spherical structure with a diameter of 800 nm approximately, and the structure of Pt/$Ti_{0.9}Mo_{0.1}O_2$ was nearly identical to the $Ti_{0.9}Mo_{0.1}O_2$ after 5% Pt was loaded on the support (Fig. 2a). To get a better view of the dispersion of the Pt particles, the transmission electron microscopy (TEM) in association with energy-dispersive X-ray spectroscopy (EDS) was employed. Fig. 2b presents a high resolution TEM (HRTEM) image of Pt/$Ti_{0.9}Mo_{0.1}O_2$, in which Pt nanoparticles about 2−3 nm were well dispersed on the support. The obvious lattice fringe with a spacing of 0.23 nm was measured as shown in the inset of Fig. 2b, which was corresponding to the (111) plane of the Pt. The homogeneous distribution of Pt, Ti, Mo and O species further proved the well dispersion of the Pt catalyst as shown by EDS mapping in Figs. 2c–h.

X-ray photoelectron spectroscopy (XPS) was further carried out to evaluate the electronic interaction between Pt and $Ti_{0.9}Mo_{0.1}O_2$. The survey spectrum of Pt/$Ti_{0.9}Mo_{0.1}O_2$ was shown in Fig. S3a (Supporting information), which proved the existence of Pt, Ti, Mo, O, and C elements, and this result was consistent with the EDS analysis. The high-resolution Mo 3d spectrum (Fig. S3b in Supporting information) can be deconvoluted into four peaks, which are attributed to Mo^{4+} and Mo^{6+}, respectively. As shown in

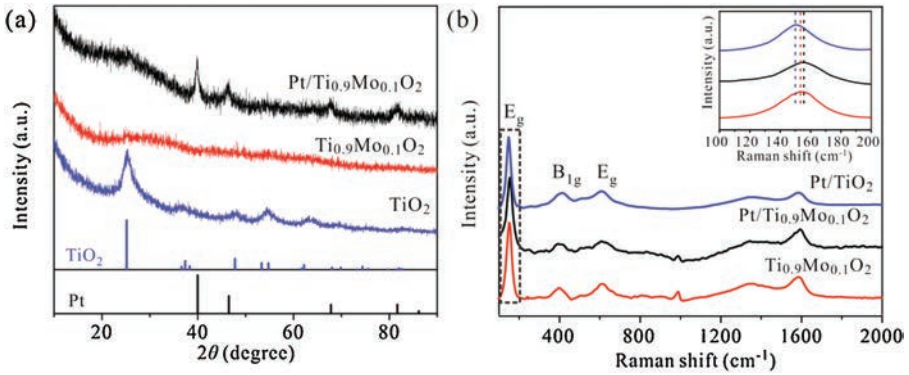

Fig. 1. (a) XRD patterns of Pt/$Ti_{0.9}Mo_{0.1}O_2$, $Ti_{0.9}Mo_{0.1}O_2$ and TiO_2. (b) Raman spectra of Pt/$Ti_{0.9}Mo_{0.1}O_2$, $Ti_{0.9}Mo_{0.1}O_2$ and Pt/TiO_2 composite. Inset: the magnification of the selected area.

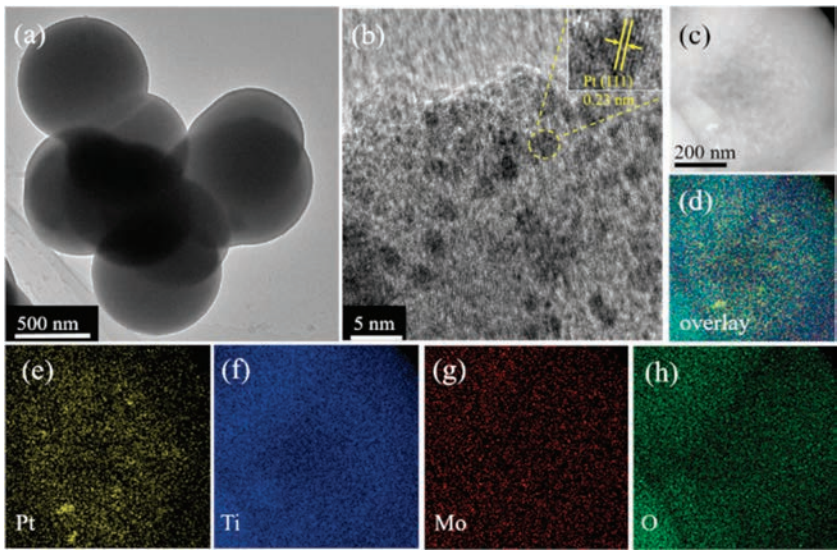

Fig. 2. (a) TEM images of $Ti_{0.9}Mo_{0.1}O_2$ and (b) HRTEM images of $Pt/Ti_{0.9}Mo_{0.1}O_2$, inset: the magnification of the selected area in yellow circle. (c–h) Elemental mapping of $Pt/Ti_{0.9}Mo_{0.1}O_2$.

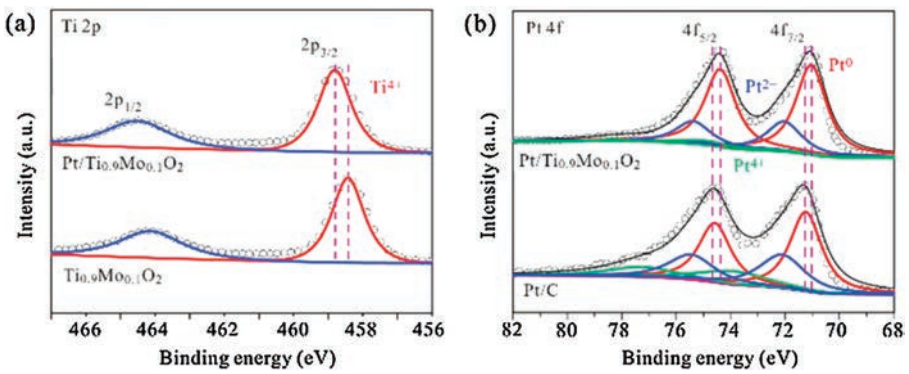

Fig. 3. (a) Ti 2p and (b) Pt 4f high-resolution XPS spectra of the $Pt/Ti_{0.9}Mo_{0.1}O_2$ catalyst.

Fig. 3a, the Ti 2p spectrum shows doublet peaks at 458.8 and 464.6 eV, demonstrating the existence state of Ti^{4+} in the catalyst. An obvious positive shift of Ti^{4+} $2p_{3/2}$ orbitals was observed towards higher binding energy relative to that of $Ti_{0.9}Mo_{0.1}O_2$, which is possibly due to the electronic interaction between Pt and $Ti_{0.9}Mo_{0.1}O_2$. Fig. 3b presents the Pt 4f core level spectra of $Pt/Ti_{0.9}Mo_{0.1}O_2$ and Pt/C. The two main peaks located at binding energy of 71.1 eV and 74.4 eV can be attributed to the $4f_{7/2}$ and $4f_{5/2}$ orbitals of Pt^0, respectively. Indeed, the existence of Pt^{2+} and Pt^{4+} species in both $Pt/Ti_{0.9}Mo_{0.1}O_2$ and Pt/C is due to the inevitable oxidation of Pt when exposed to air. The binding energy for Pt^0 $4f_{7/2}$ exhibits 0.25 eV lower relative to that of Pt/C, indicating electron donation from the $Ti_{0.9}Mo_{0.1}O_2$ to Pt. It is suggested that the interaction between the $Ti_{0.9}Mo_{0.1}O_2$ support and Pt obviously changed the electronic structure of Pt, which is possibly beneficial to the catalytic performance [35,36].

To investigate the electrocatalytic performance of these catalysts towards HER, the electrochemical characterizations were performed in 0.5 mol/L H_2SO_4. Pt/TiO_2, homemade 5% and 20% Pt/C were also performed for comparison. It can be observed in Fig. S4 (Supporting information) that the Pt/TiO_2 exhibits much lower current density because of its low electric conductivity. However, the $Pt/Ti_{0.9}Mo_{0.1}O_2$ shows a greater current density as a result of improved conductivity by Mo doping. The current improvement phenomenon can also be observed when compared with Pt/MoO_2 in Fig. S5a (Supporting information), which is assigned to weaker interaction between Pt and MoO_2. Furthermore, both 5% $Pt/Ti_{0.9}Mo_{0.1}O_2$ and 20% Pt/C show small overpotentials (26 mV and 29 mV, respectively) in the polarization curves as shown in Fig. 4a, indicating all these catalysts are highly efficient for HER. Normalized to the Pt loading, the calculated mass specific activity was compared at different over-potentials in Fig. 4b. The mass activity of 1.72 A/mg_{Pt} for 5% $Pt/Ti_{0.9}Mo_{0.1}O_2$ at an overpotential of 50 mV is 4.4-fold higher than that of 20% Pt/C (0.39 A/mg_{Pt}). It could be inferred that $Pt/Ti_{0.9}Mo_{0.1}O_2$ exhibits a better Pt utilization than Pt/C, which could effectively decrease the catalyst cost. The Tafel slope for the $Pt/Ti_{0.9}Mo_{0.1}O_2$ and 20% Pt/C were calculated in Fig. 4c with close values (36 mV/dec and 30 mV/dec, respectively), illustrating a similar reaction mechanism.

Cyclic voltammetry (CV) tests were performed in 0.5 mol/L H_2SO_4 solution. Obvious redox peaks between 0.44 V and 0.62 V can be shown in the CV profiles of $Pt/Ti_xMo_{1-x}O_2$ in Fig. S6a (Supporting information). These peaks are attributed to the formation of hydrogen molybdenum bronzes [37,38]. It is known to all that MoO_y could absorb the hydrogen and forms H_xMoO_y [19] in the presence of noble metals. The CV of $Pt/Ti_{0.9}Mo_{0.1}O_2$ in Fig. S4 (Supporting information) did not show these peaks because the Mo content is too low in the catalyst to show this characteristic. This revealed that the $Ti_{0.9}Mo_{0.1}O_2$ support is electrochemical inert under the operating condition. This results can be further proved by the comparison in Fig. S6b (Supporting information), the $Pt/Ti_{0.9}Mo_{0.1}O_2$ exhibited the best HER performance among the catalyst with different Mo content.

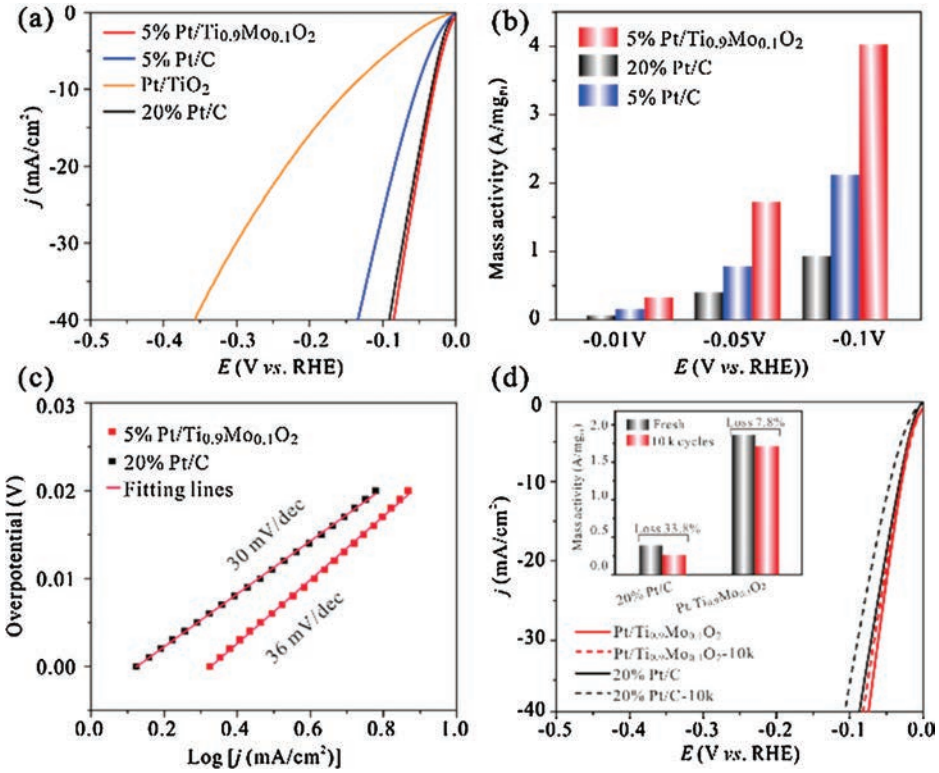

Fig. 4. (a) HER polarization curves for $Pt/Ti_{0.9}Mo_{0.1}O_2$, 20% Pt/C and Pt/TiO_2 in 0.5 mol/L H_2SO_4. Scan rate: 5 mV/s and rotating rate: 1600 rpm. (b) Comparison of the mass specific activities of $Pt/Ti_{0.9}Mo_{0.1}O_2$ and 20% Pt/C at various overpotentials. (c) Corresponding Tafel plots of polarization curves. (d) The polarization curves for $Pt/Ti_{0.9}Mo_{0.1}O_2$ and 20% Pt/C before and after the stability test. Inset: The mass specific activities of $Pt/Ti_{0.9}Mo_{0.1}O_2$ and 20% Pt/C before and after the stability test at an overpotential of 50 mV.

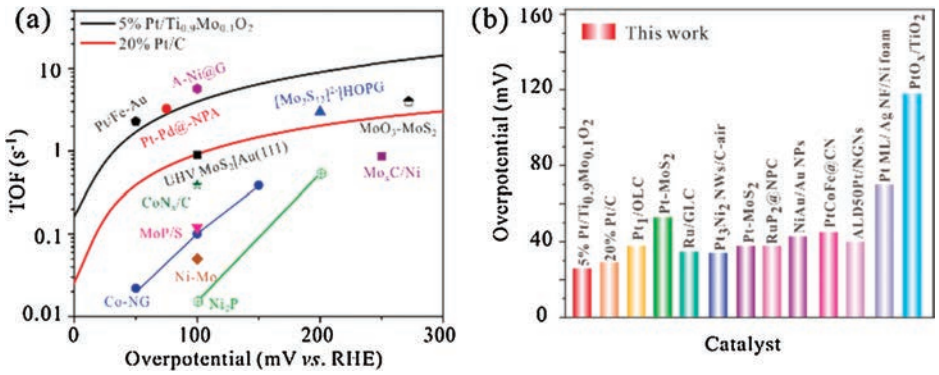

Fig. 5. Comparison of (a) TOF and (b) overpotentials at 10 mA/cm^2 of 20% Pt/C and $Pt/Ti_{0.9}Mo_{0.1}O_2$ with several HER electrocatalysts in recent literatures in 0.5 mol/L H_2SO_4.

The durability of the $Pt/Ti_{0.9}Mo_{0.1}O_2$ catalyst was evaluated *via* the accelerated degradation tests (ADT) by applying 10,000 continuous cyclic voltammetry cycles between −0.15 V and 0.4 V (*vs.* RHE) at a scan rate of 100 mV/s. It can be observed in Fig. 4d that the polarization curve of $Pt/Ti_{0.9}Mo_{0.1}O_2$ after the ADT was almost the same with the fresh catalyst, only 7.8% current density loss was seen compared with the initial value at an overpotential of 50 mV *vs.* RHE (inset in Fig. 4d). However, the Pt/C suffered from 33.8% current density loss, which demonstrated excellent durability of the $Pt/Ti_{0.9}Mo_{0.1}O_2$ catalyst. The SMSI between the $Ti_{0.9}Mo_{0.1}O_2$ support and Pt attributed to the enhanced stability as the particle migration and agglomeration were inhibited during the cycling test.

To better understand the performance of the catalysts, the turn over frequency (TOF) were also calculated, which is particular illustrated in Supporting information. Fig. 5a shows the TOF values of 5% $Pt/Ti_{0.9}Mo_{0.1}O_2$ and 20% Pt/C along with other recently reported HER catalysts. The TOF values of $Pt/Ti_{0.9}Mo_{0.1}O_2$ at 50 mV and 100 mV were 1.70 H_2/s and 3.98 H_2/s. It is obvious that $Pt/Ti_{0.9}Mo_{0.1}O_2$ exhibited greater TOF values than Pt/C and most of other catalyst at various overpotential. Moreover, the overpotential at 10 mA/cm^2 of 5% $Pt/Ti_{0.9}Mo_{0.1}O_2$, 20% Pt/C, 5% Pt/C and other recently reported noble metal HER catalyst were summarized in Table S1 (Supporting information). To achieve 10 mA/cm^2 current density, the 5% $Pt/Ti_{0.9}Mo_{0.1}O_2$ requires only 26 mV overpotential as shown in Fig. 5b. These results imply the excellent performance of $Pt/Ti_{0.9}Mo_{0.1}O_2$ with smaller overpotential compared with majority of the reported noble metal based HER catalyst.

To understand the improvement of catalytic performance, we proposed a reaction mechanism based on the hydrogen spillover effect [33] (Fig. 6), where the adsorbed H atom on the surface of Pt may easily migrate to $Ti_{0.9}Mo_{0.1}O_2$. It consists of three steps: (i) A

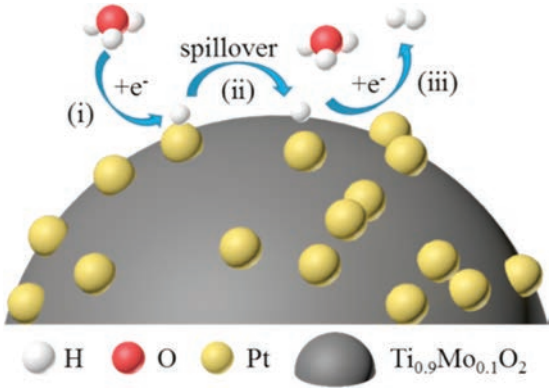

Fig. 6. The schematic illustration of the HER mechanism on $Pt/Ti_{0.9}Mo_{0.1}O_2$ catalyst.

hydronium ion adsorbs on the Pt surface combines an electron to form an adsorbed H atom; (ii) the neutral adsorbed-H atom migrates to the $Ti_{0.9}Mo_{0.1}O_2$ surface due to the spillover effect; and (iii) such H atom combines another hydronium ion and an electron to release hydrogen gas. The whole HER process may be described as following equation. It was reported that hydrogen insertion/extraction behavior is likely to be accelerated through the hydrogen spillover effect [11], the adsorption of H atom is completed on Pt surface with stronger adsorption capacity while desorption process is achieved on $Ti_{0.9}Mo_{0.1}O_2$ surface with stronger desorption capacity, which is beneficial for the HER process (reactions 1–3).

$$Pt/Ti_{0.9}Mo_{0.1}O_2 + H_3O^+ + e^- \leftrightarrow H\text{-}Pt/Ti_{0.9}Mo_{0.1}O_2 + H_2O \quad (1)$$

$$H\text{-}Pt/Ti_{0.9}Mo_{0.1}O_2 \leftrightarrow Pt/Ti_{0.9}Mo_{0.1}O_2\text{-}H \quad (2)$$

$$Pt/Ti_{0.9}Mo_{0.1}O_2\text{-}H + H_3O^+ + e^- \leftrightarrow H_2 + Pt\text{-}Ti_{0.9}Mo_{0.1}O_2 + H_2O \quad (3)$$

In summary, we have synthesized Mo-doped titanium oxide ($Ti_{0.9}Mo_{0.1}O_2$) as support for Pt nanoparticles. It is convincing that the $Ti_{0.9}Mo_{0.1}O_2$ support effectively improves the durability of the catalyst owing to the strong interaction between support and Pt. As expected, such catalyst delivers remarkable HER activity with only 26 mV overpotential, moreover, it shows 4.4 times higher mass activity than Pt/C at an overpotential of 50 mV. The excellent performance of $Pt/Ti_{0.9}Mo_{0.1}O_2$ is ascribed to the SMSI effect and the hydrogen spillover effect. The SMSI effect regulates the electronic structure of the Pt and the hydrogen spillover effect accelerates the hydrogen evolution process. This work is anticipated to provide a new idea to apply this support effect to electrocatalytic systems.

Declaration of competing interest

The authors declare that they have no known competing financial interests or personal relationships that could have appeared to influence the work reported in this paper.

Acknowledgments

This work was supported by the National Natural Science Foundation of China (No. 91963109) and the Innovation Research Funds of Huazhong University of Science and Technology (No. 2017KFYXJJ164). The authors thank the Analytical and Testing Center of HUST for its help and allowing the use of facilities for XRD, SEM and TEM.

Appendix A. Supplementary data

Supplementary material related to this article can be found, in the online version, at doi:https://doi.org/10.1016/j.cclet.2020.05.030.

References

[1] G.W. Crabtree, M.S. Dresselhaus, M.V. Buchanan, Phys. Today 57 (2004) 39–44.
[2] M.S. Dresselhaus, I.L. Thomas, Nature 414 (2001) 332–337.
[3] J.A. Turner, Science 305 (2004) 972–974.
[4] T. Huang, T. Shen, M.X. Gong, et al., Chin. J. Catal. 40 (2019) 1867–1873.
[5] X.X. Chen, X.J. Zhen, H.Y. Gong, et al., Chin. Chem. Lett. 30 (2019) 681–685.
[6] Q.B. Liu, L. Du, G.T. Fu, et al., Adv. Energy Mater. 9 (2018) 1803040.
[7] C. Cui, R.F. Cheng, C. Zhang, et al., Chin. Chem. Lett. 31 (2020) 988–991.
[8] D. Zhou, B. Jiang, R. Yang, et al., Chin. Chem. Lett. 31 (2020) 1540–1544.
[9] S. Nong, W. Dong, J. Yin, et al., J. Am. Chem. Soc. 140 (2018) 5719–5727.
[10] L. Nie, D.H. Mei, H.F. Xiong, et al., Science 358 (2017) 1419–1423.
[11] J. Park, S. Lee, H.E. Kim, et al., Angew. Chem. Int. Ed. 131 (2019) 16184–16188.
[12] J.M. Kim, Y.J. Lee, S.H. Kim, et al., Nano Energy 65 (2019) 104008.
[13] H. Li, X.F. Weng, Z.Y. Tang, et al., ACS Catal. 8 (2018) 10156–10163.
[14] J. Li, H. Zhou, H. Zhuo, et al., J. Mater. Chem. A 6 (2018) 2264–2272.
[15] J.H. Kim, S. Chang, Y.T. Kim, Appl. Catal. B: Environ. 158-159 (2014) 112–118.
[16] Y. Ji, Y.I. Cho, Y. Jeon, et al., Appl. Catal. B: Environ. 204 (2017) 421–429.
[17] U. Caudillo-Flores, M.J. Muñoz-Batista, M. Fernández-García, et al., Appl. Catal. B: Environ. 238 (2018) 533–545.
[18] L.P. Qin, G.J. Wang, Y.W. Tan, Sci. Rep. 8 (2018) 16198.
[19] R.A.M. Esfahani, S.K. Vankova, A.H.A.M. Videla, et al., Appl. Catal. B: Environ. 201 (2017) 419–429.
[20] A.D. Duma, Y.C. Wu, W.N. Su, et al., ChemCatChem 10 (2018) 1155–1165.
[21] Y. Jeon, Y. Ji, Y.I. Cho, et al., ACS Nano 12 (2018) 6819–6829.
[22] J.Y. Wang, M. Xu, J.Q. Zhao, et al., Appl. Catal. B: Environ. 237 (2018) 228–236.
[23] B.Y. Xia, S.J. Ding, H.B. Wu, et al., RSC Adv. 2 (2012) 792–796.
[24] B.Y. Xia, B. Wang, H.B. Wu, et al., J. Mater. Chem. 22 (2012) 16499–16505.
[25] K.W. Park, K.S. Seol, Electrochem. Commun. 9 (2007) 2256–2260.
[26] R.V. Genova-Koleva, F. Alcaide, G. Álvarez, et al., J. Energy Chem. 34 (2019) 227–239.
[27] R.A.M. Esfahani, L.M.R. Gavidia, G. García, et al., Renew. Energy 120 (2018) 209–219.
[28] D.L. Wang, C.V. Subban, H.S. Wang, et al., J. Am. Chem. Soc. 132 (2010) 10218–10220.
[29] V.T. Thanh Ho, K.C. Pillai, H.L. Chou, et al., Energy Environ. Sci. 4 (2011) 4194–4200.
[30] M.T. Anwar, X.H. Yan, S.Y. Shen, et al., Int. J. Hydrogen Energy 42 (2017) 30750–30759.
[31] M.C. Tsai, T.T. Nguyen, N.G. Akalework, et al., ACS Catal. 6 (2016) 6551–6559.
[32] J.J. Li, Q.Q. Guan, H. Wu, et al., J. Am. Chem. Soc. 141 (2019) 14515–14519.
[33] Y.F. Cheng, S.K. Lu, F. Liao, et al., Adv. Funct. Mater. 27 (2017) 1700359.
[34] N. Doudin, S.F. Yuk, M.D. Marcinkowski, et al., ACS Catal. 9 (2019) 7876–7887.
[35] X. Cheng, Y.H. Li, L.R. Zheng, et al., Energy Environ. Sci. 10 (2017) 2450–2458.
[36] R.A.M. Esfahani, I.I. Ebralidze, S. Specchia, et al., J. Mater. Chem. A 6 (2018) 14805–14815.
[37] P.A. Zosimova, A.V. Smirnov, S.N. Nesterenko, et al., J. Phys. Chem. C 111 (2007) 14790–14798.
[38] P. Justin, G. Ranga Rao, Int. J. Hydrogen Energy 36 (2011) 5875–5884.